U.S. Department of Commerce
National Oceanic and Atmospheric Administration
National Weather Service
National Centers for Environmental Prediction
5200 Auth Road
Camp Springs, MD 20746-4304

Office Note 433

RADIATIVE UPPER BOUNDARY CONDITIONS FOR A NONHYDROSTATIC ATMOSPHERE

R. James Purser*

Sajal K. Kar†
Environmental Modeling Center

May 2001

* General Sciences Corporation, Beltsville, Maryland; email: jpurser@ncep.noaa.gov

† UCAR Visiting Scientist Program. On leave from the Bureau of Meteorology Research Centre, Melbourne, Australia; email: skar@ncep.noaa.gov

Abstract

A nonhydrostatic compressible model supports vertically propagating acoustic modes in addition to the modes of meteorological significance, such as the quasi-geostrophically balanced, and gravity modes. The acoustic modes are stimulated inadvertently, either by initial conditions incompatibly balanced for the model discretization, or by physical processes injecting abrupt impulses of heat or motion into the model during the integration. A standard method for removing unwanted acoustic energy is through the inclusion in the model of three-dimensional divergence damping. However, an alternative approach is to employ an upper boundary condition designed to radiate acoustic waves, at least partially, as they impinge on the model top. This note explores this latter option through the use of an upper boundary condition that incorporates a time filter facilitate the selective absorption of both gravity and acoustic waves at the top.

1. Introduction

For a numerical weather prediction model with a finite top, the upper boundary becomes a potential source of spurious reflected gravity waves if precautions are not taken to dissipate them or let them pass through. In a nonhydrostatic model the problem is exacerbated by the additional presence of acoustic modes. The gravity waves are generated at significant amplitude by realistic meteorological processes, such as orographic or convective forcing. The acoustic modes are only produced accidently by poor initialization or noisy parameterizations, but unless measures are taken to control them, the reverberating acoustic modes can build up and overwhelm the numerics of the model over the course of an extended integration. Even a weak absorption of the acoustic modes is sufficient to control them and prevent the potential instability that they might otherwise cause. Three-dimensional divergence damping is often adopted, although this cure can inadvertently affect the slower gravity modes too. While a 'sponge layer' (e.g., Klemp and Lilly 1978) occupying the top portion of the model is effective in absorbing both kinds of modes, it can be a wasteful solution because it contaminates that portion of the model grid with dynamical effects that are not faithful to the intended governing equations. A more satisfactory solution would be to leave the interior equations unaltered and to specify what is usually referred to as a 'radiative boundary condition' at the top. This is a set of constraints on the model variables, affecting directly only quantities stored in the top one or two levels, that causes the impinging waves to behave *as if* the model atmosphere continued, without interruption by the actual boundary, up into the space beyond *. For any model it is desirable that the radiative upper boundary condition be highly efficient for gravity waves, that is, producing little or no reflection, since the alternative measures by which the amplitudes of such reflected waves can be controlled (such as the sponge layer) invariable affect their physically realistic upward-propagating counterparts adversely. However, In the case of a nonhydrostatic model, it is also desirable that the condition be at least partially

* Given that no actual 'radiation' occurs, the more accurately descriptive 'non-reflecting boundary condition' is probably a better phrase to use.

effective at suppressing the reflections of the acoustic modes that reach the top, although, being meteorologically unimportant, alternative suppression techniques like divergence damping and time filtering for these modes have no need to discriminate the upward and downward propagating waves. Engquist and Majda (1977) provide approximate boundary conditions for the classical wave equation, which could in principle apply to the high-frequency acoustic waves. The problem of applying radiative boundary conditions to dispersive gravity and Rossby waves is examined by Bennett (1976) and by Beland and Warn (1975), who employ Laplace and Fourier transforms to show that exact conditions require a nonlocal treatment in both space and time. On this basis, it is doubtful that any practical (finite memory) boundary conditions of even a linear model can prevent the reflection of gravity or Rossby waves entirely. For Hydrostatic internal gravity waves a solution that is local in time, but nonlocal in space, is available in the form of the conditions independently proposed by Bougeault (1983) and by Klemp and Durran (1983). These methods have been generalized by Garner (1986) to include a Coriolis effect and by Rasch (1986) to treat large scale Rossby waves. A review of these and other methods is given by Givoli (1991).

We seek to obtain inexpensive upper boundary conditions that are not only efficient at radiating nonhydrostatic gravity waves but which simultaneously radiate (if only inefficiently) any vertically or obliquely propagating acoustic modes supported by a nonhydrostatic compressible model. We suggest that radiative boundary conditions employing recursive time filters of at least second order should be able to reduce the degree of spurious reflection of gravity waves to a level that is sufficient for most practical purposes while simultaneously causing the amplitude of acoustic noise to diminish well within the time scales typical of numerical predictions. The suggested method, which can be thought of as generalizing the boundary condition of Bougeault (1983) and Klemp and Durran (1983) to the nonhydrostatic compressible domain, is described. Further generalizations to incorporate the effects of rotation and varying stratification would seem to be possible but are not developed in the present paper.

2. Perturbation equations for an isothermal basic state at rest

(*a*) *Basic variables*

We shall assume the basic state consists of air at a constant temperature T_0 at rest and in hydrostatic equilibrium with a constant gravitational acceleration g. We assume no rotation. As usual, we take the specific heats at constant pressure and at constant volume and the gas constant to be in the ratio:

$$(C_p : C_v : R) = (7 : 5 : 2),$$

and define numerical constants, $\gamma = C_p/C_v = 7/5$ and $\kappa = (\gamma - 1)/\gamma = 2/7$. Other important constants for the given basic state are: $c = \sqrt{\gamma R T_0}$, the speed of sound; $H = RT_0/g$, the atmospheric scale height; $N = \sqrt{\kappa/\gamma}c/H$, the Brunt-Väisälä frequency. In this study, we shall choose, in SI units: $R = 287$; $T_0 = 273$; $g = 9.81$. Then,

$$\begin{aligned} c &\approx 331, \\ N &\approx .0187, \\ H &\approx 7987. \end{aligned}$$

In a two-dimensional vertical slice, we let u and w be the horizontal and vertical wind components. T is the temperature, P is the pressure, $\rho = P/RT$ is the density. For convenience, we use a constant reference pressure, P_{00}, to define the Exner function and potential temperature:

$$\pi = C_p(P/P_{00})^{\kappa},$$

$$\theta = C_p T/\pi.$$

Then the basic state's Brunt-Väisälä frequency can be expressed equivalently:

$$N = \{g(\partial\theta_0/\partial z)/\theta_0\}^{1/2}.$$

(*b*) *The basic state*

We use a zero suffix to denote the basic state variables. The hydrostatic balance for the basic state is:

$$\theta_0 \frac{\partial \pi_0}{\partial z} = -g.$$

Combining this with the identity,

$$\theta_0 = C_p T_0/\pi_0,$$

we find the exponential forms of the vertical profiles of the principal basic state variables:

$$\pi_0 = C_p \exp\left(\frac{-gz}{C_p T_0}\right) \equiv C_p \left[\exp\left(\frac{-z}{H}\right)\right]^{\kappa}, \tag{2.1}$$

$$\rho_0 = \frac{P_{00}}{RT_0} \exp\left(\frac{-z}{H}\right), \tag{2.2}$$

$$P_0 = P_{00} \exp\left(\frac{-z}{H}\right), \tag{2.3}$$

$$\theta_0 = T_0 \left[\exp\left(\frac{z}{H}\right)\right]^{\kappa}. \tag{2.4}$$

(*c*) *Perturbation equations*

About this basic state, the equations for perturbations are:

$$\begin{aligned}
\frac{\partial u}{\partial t} &= -\theta_0 \frac{\partial \pi}{\partial x}, \\
\frac{\partial w}{\partial t} &= -\theta_0 \frac{\partial \pi}{\partial z} + g\frac{\theta}{\theta_0}, \\
\frac{\partial \pi}{\partial t} &= -(\gamma - 1)\pi_0 \left(\frac{\partial u}{\partial x} + \frac{\partial w}{\partial z}\right) + g\frac{w}{\theta_0}, \\
\frac{\partial \theta}{\partial t} &= -wN^2 \frac{\theta_0}{g}
\end{aligned}$$

But if we adopt the rescaling:

$$\begin{aligned} u &\leftarrow \rho_0^{1/2} u, \\ w &\leftarrow \rho_0^{1/2} w, \\ \pi &\leftarrow \left(\frac{\rho_0^{1/2}\theta_0}{c}\right)\pi, \\ \theta &\leftarrow \left(\frac{g\rho_0^{1/2}}{\theta_0 N}\right)\theta, \end{aligned}$$

then the perturbation equations become more symmetrical:

$$\frac{\partial u}{\partial t} = -c\frac{\partial \pi}{\partial x}, \tag{2.5}$$

$$\frac{\partial w}{\partial t} = -c\left(\frac{\partial}{\partial z} + \frac{1}{L}\right)\pi + N\theta, \tag{2.6}$$

$$\frac{\partial \pi}{\partial t} = -c\frac{\partial u}{\partial x} - c\left(\frac{\partial}{\partial z} - \frac{1}{L}\right)w, \tag{2.7}$$

$$\frac{\partial \theta}{\partial t} = -Nw, \tag{2.8}$$

where $L = 14H/3 \equiv 14RT_0/(3g)$ can be denoted the *Lamb-height* since it is the e-folding distance for the Lamb wave perturbation, in units for which the energy density scales as the square of the perturbation. The energy density becomes half the integrated sum of squares of these new perturbation variables.

3. Designing boundary conditions

(*a*) *Dispersion relations and wave impedance*

Assume $\frac{\partial}{\partial x} \equiv ik$ for a horizontal Fourier harmonic. Then assume all the dependent variables scale like:

$$\psi = \tilde{\psi} e^{st}, \tag{3.1}$$

for some nonvanishing complex s with positive real part, $\Re(s) > 0$. Our original equations then become:

$$\begin{aligned} s\tilde{u} &= -ick\tilde{\pi}, \\ s\tilde{w} &= -c\mathcal{D}\tilde{\pi} + N\tilde{\theta}, \\ s\tilde{\pi} &= -ick\tilde{u} - c\mathcal{D}^*\tilde{w}, \\ s\tilde{\theta} &= -N\tilde{w}. \end{aligned}$$

where,

$$\mathcal{D} \equiv \left(\frac{d}{dz} + \frac{1}{L}\right),$$

$$\mathcal{D}^* \equiv \left(\frac{d}{dz} - \frac{1}{L}\right).$$

Applying substitutions,

$$\tilde{u} = \frac{-ick}{s}\tilde{\pi},$$
$$\tilde{\theta} = \frac{-N}{s}\tilde{w},$$

we obtain:

$$\left(\frac{N^2}{s} + s\right)\tilde{w} = -c\mathcal{D}\tilde{\pi}, \tag{3.2}$$
$$\left(\frac{c^2k^2}{s} + s\right)\tilde{\pi} = -c\mathcal{D}^*\tilde{w}, \tag{3.3}$$

or the single equation for $\tilde{\pi}$:

$$\tilde{\pi} = K^2\mathcal{D}^*\mathcal{D}\tilde{\pi}, \tag{3.4}$$

where

$$K^2 = \frac{s^2c^2}{(N^2+s^2)(c^2k^2+s^2)}. \tag{3.5}$$

For the case of a definite exponential growth of the solution in time, $\Re(s) > 0$, any characteristic solution corresponding to forcing only from below has state variables exhibiting vertical profiles like:

$$\tilde{\pi} = \tilde{\pi}^+ e^{-\mu z},$$

where μ, which is complex in general, has $\Re(\mu) > 0$. This corresponds to the exponential decay in height that must accompany exponential growth in time for the assumption of forcing from below to make physical sense in homogeneous, passive medium with finite propagation speeds for wave disturbances. For solutions of pure oscillatory form in time, $\Re(s) = 0$, the more familiar constant-amplitude wave solutions of the dispersion relation, with $\Re(\mu) = 0$ can also exist. Note that,

$$\mathcal{D}\mathcal{D}^* \equiv \left(\frac{d^2}{dz^2} - \frac{1}{L^2}\right),$$

so the dispersion relation can be expressed,

$$\mu^2 = \left(\frac{1}{L^2} + \frac{1}{K^2}\right).$$

For later algebraic convenience, we note that,

$$s^2c^2\mu^2 = N^2c^2k^2 + s^2c^2\left(k^2 + \frac{1}{4H^2}\right) + s^4.$$

From (3.2) and (3.3),

$$\tilde{\pi} = \hat{Z}\tilde{w}, \tag{3.6}$$

where,

$$\hat{Z}(s) = \frac{sc}{c^2k^2+s^2}\left(\mu + \frac{1}{L}\right) \equiv \frac{1}{c^2k^2+s^2}\left(\left[N^2c^2k^2 + s^2c^2\left(k^2 + \frac{1}{4H^2}\right) + s^4\right]^{1/2} + \frac{sc}{L}\right), \tag{3.7}$$

is sometimes referred to, in the terminology of general wave propagation theory (e.g., Morse and Feshbach 1953, p. 128), as the characteristic 'impedance' at this s and k.

(b) *Upper boundary impedance conditions*

Suppose the condition at the upper boundary, which we shall conveniently locate at $z = 0$, is written:

$$\pi(t) = \int_0^\infty Z(t')w(t-t')dt'. \tag{3.8}$$

That is, a lagged superposition of 'effects' π depending on only *preceding* 'causes' w through a convolution with the impedance kernel $Z(t')$, with $Z(t') = 0$ for $t' < 0$. Use Laplace transforms to express:

$$\begin{aligned} \pi(t) &= \int_0^\infty \tilde{\pi} e^{st} ds, \\ w(t) &= \int_0^\infty \tilde{w} e^{st} ds, \end{aligned}$$

so that,

$$\tilde{\pi}(s) = \int_0^\infty Z(t')e^{-st'}dt'\ \tilde{w}(s). \tag{3.9}$$

Hence, inverting the relation,

$$\hat{Z}(s) = \int_0^\infty Z(t')e^{-st'}dt', \tag{3.10}$$

provides the 'perfect' radiative boundary condition for these linearized waves. Unfortunately, since the kernel, $Z(t)$ is highly structured in the t domain (despite the deceptively simple appearance of its Laplace transform) any computationally feasible approximations to $Z(t)$, expressible using only modest memory resources, inevitably incur significant errors for at least some physically relevant values of the complex parameter s. Good radiative boundary conditions seek to keep this error small in the portion of s that corresponds to the frequencies of the waves for which a significant amount of reflection would be most detrimental, while maintaining overall numerical stability.

In the absence of any special boundary condition, for example, when the vertical velocity is set to zero at the model top (corresponding to infinite impedance) all incident acoustic and gravity waves are fully reflected. A vast improvement is obtained by the choice of an impedance set equal to the asymptotic low-frequency limit:

$$\hat{Z}_0(s) = \lim_{s\to 0} \hat{Z}(s) = Z_g, \tag{3.11}$$

or,

$$Z_0(t) = Z_g \delta(0^+), \tag{3.12}$$

where the notation in (3.12) signifies that the delta function is fully included within the range of a one-sided integral like (3.8). This closely matches the impedance of the lowest-frequency gravity waves for which the nonhydrostatic effects are less significant. This impedance is a function of horizontal wavenumber simply through:

$$Z_g = \frac{N}{c|k|}. \tag{3.13}$$

Moreover, as a boundary condition, it acts instantaneously instead of involving any finite lag, so it is reasonably simple to apply in any model whose horizontal domain is of a shape that facilitates double Fourier transformation, provided the neglect of horizontal variations of N at the top can be tolerated. It is, in fact, the boundary condition proposed by Klemp and Durran (1983) and by Bougeault (1983).

We can insert $s = i\sigma$ and use (3.7) to express the *complex* impedance $\hat{Z}$ as a function of frequency σ. The two branches of complex μ, which we may denote μ^+ and μ^-, correspond to upward and downward propagating waves of the common frequency, σ. In general, both branches contribute to the solution satisfying a given boundary impedance condition. Thus, if

$$\tilde{w} = \tilde{w}^+ + \tilde{w}^-,$$

and

$$\begin{aligned} \tilde{\pi} &= \tilde{\pi}^+ + \tilde{\pi}^-, \\ &= \hat{Z}^+ \tilde{w}^+ + \hat{Z}^- \tilde{w}^-, \end{aligned}$$

then the upper boundary ($z = 0$) impedance, $\hat{Z}_b$, at a particular frequency σ establishes the ratio between $\tilde{w}^+$ and $\tilde{w}^-$ through:

$$\tilde{w}^- = \left(\frac{\hat{Z}^+ - \hat{Z}_b}{\hat{Z}_b - \hat{Z}^-} \right) \tilde{w}^+. \tag{3.14}$$

The magnitude of this ratio between the amplitudes of downward and upward waves will be referred to as the reflection coefficient:

$$R_b(\sigma) = \left| \frac{\hat{Z}^+ - \hat{Z}_b}{\hat{Z}_b - \hat{Z}^-} \right|. \tag{3.15}$$

(Note that the *square* of R_b^2 represents the proportion of wave *energy* that is reflected.) For the case, $\hat{Z}_0(\sigma) = Z_g$, and for a wave of horizontal wavelength, $\lambda = 2\pi/k = 2000$ m we obtain the reflection profiles for the gravity and acoustic modes shown in Fig. 1 by the solid curves. While this method is reasonably good for gravity waves, especially in the hydrostatic and high vertical wavenumber limit, $s \to 0$, where the reflection coefficient tends to zero, it is clear that this boundary condition does very little to absorb the acoustic modes (for which it was never originally designed). The reason is that the limiting impedance in (3.7) for purely vertically propagating acoustic waves is, in our particular choice of scaling units,

$$\lim_{s \to \infty} \hat{Z}(s) \equiv Z_a = 1,$$

which is many times larger than the magnitudes of impedances typical of atmospheric gravity waves, and the impedance of obliquely-propagating acoustic waves is even greater.

A partial solution to radiating both gravity and acoustic waves is to employ an exponentially-lagged time filter to retain a 'memory' of recent vertical velocity at the top:

$$\bar{w}(t) = \int_0^\infty r e^{-rt'} w(t - t')\, dt', \tag{3.16}$$

and then to use this for the upper boundary condition:

$$\pi(t) = Z_a w(t) - (Z_a - Z_g)\bar{w}(t). \tag{3.17}$$

An operator whose effect is the discretization of the smoothing integral (3.16) is obtained by applying a first order recursive filter that solves the backward-difference analogue of the differential equation:

$$\frac{d\bar{w}}{dt} = -r(\bar{w} - w). \tag{3.18}$$

(For a more detailed discussion of recursive filters and their connection with linear homogeneous difference equations, see Hamming 1989, Chap. 12.) The impedance implied by this new boundary condition is

$$\hat{Z}_1 = Z_a - \frac{(Z_a - Z_g)r}{r + s}. \tag{3.19}$$

The choice of the smoothing rate, r, can be used to trade off the quality of the radiation condition for gravity modes against the quality of treatment for the acoustic modes. For an intermediate value, $r = 2.\ \mathrm{s}^{-1}$ (a time scale of about half a second), the dotted curves of Fig. 1 show the reflection coefficient obtained with horizontal wave length $\lambda = 2000$ m. For acoustic waves propagating in the strictly vertical direction the new boundary condition is now efficiently absorbing but, compared with the Klemp and Durran condition, the treatment of gravity waves is now made rather worse. Evidently, the first-order filtering approach does not constitute a completely satisfactory solution.

In a meteorological simulation, the acoustic waves are generated accidently either through improper specification of initial conditions, or continuously through acoustically noisy parameterization of physical processes. There is no significant generation of acoustic waves by real meteorological processes. Because of their rapid speed, the vertically and obliquely propagating acoustic modes reverberate between upper and lower boundaries many times per hour, providing numerous opportunities for their absorption. Therefore, in selecting an upper boundary condition, we should perhaps not devote too much effort to the efficient radiation of the acoustic modes when even an inefficient upper boundary condition can be enough to remove them quickly from the model. A more cost-effective approach to refining the boundary conditions is to conform the boundary impedance more closely to the profile (in s) of the impedance of the upward propagating gravity wave in the vicinity of $s = 0$. To this end, we consider refining the definition of $\bar{w}$ in (3.17) by the substitution of a second-order recursive filter. Since the slope, $d\hat{Z}/ds$, is very small at $s = 0$ for most modes we may obtain a good local fit using a filter for which the slope at $s = 0$ is exactly zero and the curvature component, $d^2\hat{Z}/ds^2$, at $s = 0$ implied by the filter closely matches that implied by (3.7). The impedances implied by second-order recursive filter formulations are second-degree rational functions. Our requirements are met by the form,

$$\hat{Z}_2 = Z_a - \frac{(Z_a - Z_g)(2bs + r^2)}{s^2 + 2bs + r^2}. \tag{3.20}$$

(The neglected finite slope term can be accommodated by changing the numerator term, $2bs$, to something more appropriate, but the algebraic complexity involved in satisfying the additional condition is not trivial.) Such a filter is provided by recursively solving the numerical

representation of:

$$\frac{d^2\bar{w}}{dt^2} = -2b\left(\frac{d\bar{w}}{dt} - \frac{dw}{dt}\right) - r^2(\bar{w} - w). \tag{3.21}$$

The impedance $\hat{Z}_2$ retains the desirable asymptotic limits,

$$\begin{aligned} \lim_{s\to 0} \hat{Z}_2 &= Z_g, \\ \lim_{s\to\infty} \hat{Z}_2 &= Z_a, \end{aligned}$$

but we can select coefficients b and r^2 to obtain a better impedance match near $s = 0$. Since

$$\left.\frac{d^2\hat{Z}_2}{ds^2}\right|_{s=0} = \frac{2(Z_a - Z_g)}{r^2}, \tag{3.22}$$

and, for the actual upward-propagating gravity wave,

$$\left.\frac{d^2\hat{Z}^+}{ds^2}\right|_{s=0} = \frac{c^2[k^2 + 1/(4H^2)] - 2N^2}{N|ck|^3}, \tag{3.23}$$

we need to choose,

$$r^2 = \frac{2(Z_a - Z_g)N|ck|^3}{c^2[k^2 + 1/(4H^2)] - 2N^2}. \tag{3.24}$$

The choice of coefficient b remains undetermined, although it must be nonnegative if the filter is to remain stable. One possible choice is $b = r/\sqrt{2}$, the consequence of which is shown in the dashed curves of Fig. 1 for the same horizontal wave length selected for the other curves. It is possible to choose b more intelligently, for example, by demanding a third-order fit of the impedance profile near $s = 0$, and accounting for the presently neglected linear term, but the results of experiments in which b has been changed have not shown a great sensitivity to this parameter.

In a set of simple idealized experiments, we have numerically implemented the linearized equations for a single horizontal wave length about an isothermal rest state for an atmosphere extending to almost four kilometers. From an initial state at rest, the model is forced at the chosen horizontal wavelength with a transient pulse of positive w at the ground. The pulse has a bell-shaped time profile in piecewise polynomial segments,

$$w_0(m\tau + t) \propto \sum_{k=0}^{4} P_{m,k}(t/\tau)^k, \qquad 0 \le t \le \tau, \qquad m = 0, 1, \ldots, 4 \tag{3.25}$$

where $\tau = 10$ s, so the overall width of the profile is $5\tau = 50$ s. The fourth-degree polynomials in each segment are those associated with a uniform grid *B-spline* (de Boor 1978):

$$\begin{array}{lrrrrrr} P_{0,k} & & 0, & 0, & 0, & 0, & 1/24 \\ P_{1,k} & & 1/24, & 1/6, & 1/4, & 1/6, & -1/6 \\ P_{2,k} & \equiv & 11/24, & 1/2, & -1/4, & -1/2, & 1/4 \\ P_{3,k} & & 11/24, & -1/2, & -1/4, & 1/2, & -1/6 \\ P_{4,k} & & 1/24, & -1/6, & 1/4, & -1/6, & 1/24. \end{array} \tag{3.26}$$

This forcing stimulates bursts of both gravity and acoustic waves which are well resolved in time and in the vertical by the model. The acoustic modes rapidly reach the model top and are repeatedly reflected between the top and bottom. The more slowly propagating gravity waves take around 2000 s to reach the top. Fig. 2 shows what happens when the upper boundary impedance is tuned simply to radiate the vertically propagating acoustic waves only, $Z(t) = Z_a\delta(0^+)$. The upper panel shows plots of the vertical profile of the pressure perturbation every 18 s (except for the first few occurring during the period of bottom boundary forcing, which are omitted owing to their excessive amplitudes) over the course of a 90-minute integration. The lower panel plots the lowest-level pressure trace for the same period, again omitting the initial forcing period. The apparent thickness of the latter trace at the start is a result of the rapid acoustic oscillations which damp out fairly quickly in the subsequent integration (by about 3000 s the lowest-level pressure trace has become a thin line). A moderately coherent 'beam' of gravity waves is seen to rise to the model top where, in this experiment, it is almost completely reflected, then reflected again at the ground about an hour from the initial time. Note that the gravity waves with relatively small vertical wave lengths propagate more slowly and therefore form a pronounced interference pattern with the reflections of their faster, longer wave length counterparts.

Fig. 3 shows the same set up as in Fig. 2, but now with the upper boundary impedance, $Z(t) = Z_0 \equiv Z_g\delta(0^+)$, given by the Klemp and Durran prescription. Clearly, the acoustic modes are not significantly reduced in amplitude throughout the integration period. Their amplitude in the pressure trace is comparable to the gravity wave contribution, giving the profiles in the upper panel a rough 'wood grain' appearance. However, the gravity wave components are quite well removed by this upper boundary condition. In Fig. 4 we use the first-order filter construction for the upper boundary, in this case with filter parameter $r = 2\ \mathrm{s}^{-1}$, to obtain the boundary impedance Z_1 of (3.19). This condition with this parameter r is moderately successful in radiating both the acoustic noise (although some persists beyond one hour) and gravity waves. With a parameter $r = 0.5\ \mathrm{s}^{-1}$ (that is, implying a filter memory of longer duration) the same form of upper boundary impedance Z_1 leads to the results shown in Fig. 5, in which the acoustic noise is more efficiently radiated. However, this is clearly inferior to the choice $Z = Z_g$ of Fig. 3 when considering the gravity waves.

Replacing the first order filter by our second order filter, to obtain the boundary impedance Z_2 of (3.20) leads to a marked improvement, as shown in Fig. 6. The acoustic noise is promptly controlled and the gravity waves are very efficiently radiated, leaving only the faintest hint of a reflected wave.

Waves with shorter horizontal wavelengths tend to be more affected by nonhydrostatic effects. Our second-order filter condition applied to waves with $\lambda = 1000$ m leads to the wave evolution illustrated in Fig. 7. Note that, at this short wavelength, the acoustic modes are of a sufficiently high frequency not to be strongly stimulated by the initial forcing. The radiation condition for gravity waves is slightly less efficient than before. Conversely, choosing $\lambda = 5000$ m leads to a more prominent acoustic component initially but a more perfect radiation of the gravity waves at the top, as shown in Fig. 8. The more rapid diminution of the acoustic noise amplitude in this figure is thought to be a consequence of the fact that a greater proportion of the acoustic waves present are now more vertically oriented.

These experiments have focused on more efficiently radiating the gravity wave but it is

worth noting that one can alternatively devote the inherent *memory* of the recursive filter to the time scales more relevant to the oblique acoustic modes. For example, a reasonably snug fit to the impedance of vertically-propagating acoustic modes in the limit $s \to \infty$ is obtained with the same impedance model, (3.20), but with very small b and

$$r^2 = c^2 k^2 / 2. \tag{3.27}$$

For the wave with $\lambda = 2000$ m stimulated in the same way as in our earlier experiments, the result is shown in Fig 9. The removal of the acoustic noise is indeed noticeably more rapid and, since the limit, $\hat{Z} \to Z_g$ is preserved as $s \to 0$, we still retain a moderate standard of efficiency in the radiation of the gravity waves. However, to achieve efficient radiation for significant ranges of both acoustic and gravity waves (that is, at both ends of the frequency spectrum) using a recursive filtering technique, it would probably require a filter of not less than fourth-order to be truly effective.

4. Numerical implementation

The radiative upper boundary condition has been implemented and tested in a two-dimensional time-dependent model based on the prognostic equations given in section 2(c), that are modified to include advection by an uniform current u_0 in x. The model domain can be noncyclic in x, with appropriate open boundary conditions that are discussed later. The model grid shown in Fig. 10 is semi-staggered, with a Charney-Phillips grid in the vertical. Second-order centered differences are used for all terms, except advection for which a third-order upwind scheme is used. An explicit, fourth-order, low-storage Runge-Kutta scheme (Gill 1951) has been used for time differencing. Note that choice of the space and time difference schemes are not crucially important for this 'toy' model, primarily set up to test the upper boundary condition.

Typically, after each Runge-Kutta time step, the radiation condition (3.17) is used to diagnostically update $\pi_{i,K+1}$ in terms of w_i extrapolated to the same level. To discretize (3.18) in time, a backward difference is used leading to the scheme:

$$\bar{w}^t = \frac{r\Delta t}{1 + r\Delta t}(w^t + \bar{w}^{t-\Delta t}), \tag{4.1}$$

where Δt is the time step. For the time discretization of the second-order recursive filter (3.21), we introduce an auxiliary variable q and rewrite (3.21) as a system of two first-order ODEs:

$$\frac{d\bar{w}}{dt} = q, \tag{4.2}$$

$$\frac{dq}{dt} = -2b\left(q - \frac{dw}{dt}\right) - r^2(\bar{w} - w), \tag{4.3}$$

and then employ, once again, backward differences in time leading to the scheme:

$$(1 + 2b\Delta t)q^t + r^2 \Delta t \bar{w}^t = (q - 2bw)^{t-\Delta t} + (2b + r^2\Delta t)w^t, \tag{4.4}$$

$$-\Delta t q^t + \bar{w}^t = \bar{w}^{t-\Delta t}. \tag{4.5}$$

Note that (4.4) and (4.5) ensure a non-singular system for $(q, \bar{w})^t$ as $1 + 2b\Delta t + (r\Delta t)^2 > 0$ is always satisfied.

(a) *Linear hydrostatic mountain wave problem*

Although no surface topography is included in this 2D model, one can prescribe a stationary vertical velocity field at the lower boundary and carry out pseudo mountain wave simulations. Fortunately, analytic solutions of 2D anelastic, non-rotational flow over topography for an isothermal atmosphere with an uniform zonal flow are well established (Alaka 1960, or Smith 1979). For the bell-shaped mountain contour with the height h and the half-width a

$$z_s(x) = \frac{ha^2}{x^2 + a^2}, \tag{4.6}$$

the zonal and vertical velocity perturbations are given by

$$u = -\frac{u_0}{\rho_0}\frac{\partial}{\partial z}(\rho_0 \delta), \tag{4.7}$$

$$w = u_0 \frac{\partial \delta}{\partial x}, \tag{4.8}$$

where δ is the displacement streamline given by,

$$\delta(x, z) = \left(\frac{\rho_0}{\rho_{00}}\right)^{-\frac{1}{2}} ha \frac{a \cos mz - x \sin mz}{x^2 + a^2}, \tag{4.9}$$

$$\rho_{00} = \rho_0(z = 0), \tag{4.10}$$

and m is the Scorer parameter:

$$m = g\left(\frac{1}{C_p T_0 u_0^2} - \frac{1}{4R^2 T_0^2}\right). \tag{4.11}$$

These analytic solutions were obtained assuming a radiation upper boundary condition and that the disturbances vanish as $|x| \to \infty$.

To simulate such waves in our model, we prescribe the lower boundary condition as $u = u_0 \partial z_s / \partial x$. To mimic the open lateral boundaries used in the analytic model, we have implemented a variation of the Orlanski-type boundary condition in the model (Orlanski 1976). At the outflow boundary, first-order upwind schemes are used for the advection terms. The model domain expands over 128×25 grid points, with $\Delta x = 2$ km, $\Delta z = 250$ m. The other relevant parameters are $T_0 = 250$ °K, $u_0 = 20$ m s^{-1}, $a = 10$ km, $h = 1$ m. The basic state is characterized by $N = 0.019$ s^{-1}, $H_0 = 7.317$ km, $c = 317$ m s^{-1}. Note that $Na/u_0 \gg 1$ and $Nh/u_0 \ll 1$, so that only small-amplitude hydrostatic mountain waves are forced. The time step is 0.4 s. The nearly steady-state numerical solution for u and w at $u_0 t/a = 60$ or $t = 30,000$ s is shown in Fig. 11. The corresponding analytic solutions are also shown in the same figure. The numerical solution displayed in Fig. 11 employs the radiation condition with the second-order filter, which is practically same as the numerical solutions (not shown) obtained using the first-order filter. The numerical solutions are very close to the analytic solutions, except for the small differences in magnitudes of the maximum and minimum values. Such results compare favorably

to the similar numerical solutions shown by Durran and Klemp (1983) and others. This pseudo mountain wave experiment shows that the radiation condition is numerically stable and able to radiate out linear hydrostatic mountain waves with sufficient accuracy.

(*b*) *Transient acoustic and gravity wave problem*

In this test, transient acoustic and gravity waves are excited in the centre of the model domain using a very localized, short-lived heating profile of the form

$$Q(x,z,t) = Q_0 \exp\left[-\frac{1}{2}\left\{\left(\frac{x-x_0}{S_x}\right)^2 + \left(\frac{z-z_0}{S_z}\right)^2 + \left(\frac{t-t_0}{S_t}\right)^2\right\}\right], \tag{4.12}$$

where (S_x, S_z, S_t) denote the characteristic scales in (x, z, t) dimensions. The heating term appears as Q/C_p in the prognostic equation for q. For this experiment, a cyclic domain with a resting isothermal basic state is used. The parameters related to Q are set as $S_x = 1$ km, $S_z = 0.5$ km, $S_t = 50$ s. The model domain expands over grid points, with $\Delta x = 125$ m, $\Delta z = 100$ m with a time step of 0.2 s. While (x_0, y_0) correspond to the grid $(64, 32)$, t_0 is (subjectively) set to $18S_t$ so that the heating is not introduced as a shock. The time integration is carried out for four hours using the radiation condition with the second-order filter. Fig. 12 shows the 3D surface plots of the perturbation divergence, $D = \partial u/\partial x + \partial w/\partial z$, at $x = x_0$ as a function of height and time. After a noisy start up, we notice that vertically propagating gravity waves superimposed with smaller period acoustic waves are being absorbed gradually by the radiative upper boundary; in fact, beyond 3.5 hours, the divergence surface has become quite flat. This experiment illustrates the effectiveness and the numerical stability of the radiation condition for transient acoustic and gravity waves, as opposed to the stationary gravity wave simulations shown earlier.

5. Conclusion

This preliminary study of radiation boundary conditions for a compressible nonhydrostatic atmosphere suggests that it is indeed possible to extend the method of Bougeault (1983) and Klemp and Durran (1983) to include partial absorption of acoustic modes while improving the handling of those gravity modes significantly modified by nonhydrostatic effects. The method involves the application of a temporal recursive filter at the model top. However, first-order recursive filtering is found not to be sufficent — satisfactory results require the application of a filter of at least second order. Like the conditions of Bougeault, Klemp and Durran, the new method requires a horizontal spectral decomposition at the model top. This raises the question whether the resulting boundary condition can then accommodate horizontal variations in the Brunt-Väisälä frequency (assumed uniform in this limited study). This question needs to be addressed in a more complete model before we can give an authoritative answer. One possible approach to treating horizontal inhomogeneities in static stability is to use overlapping local approximations to the spectral decompositions, each patch using its own average value of N, then merge the resulting conditions implied for π in some smooth way.

Acknowledgment

We are grateful to Dr. Shrinivas Moorthi for valuable comments on an earlier draft of this paper. This work was partially supported by the NSF/NOAA Joint Grants Program of the US Weather Research Program. This research is also in response to requirements and funding by the Federal Aviation Administration (FAA). The views expressed are those of the authors and do not necessarily represent the official policy or position of the FAA.

References

Alaka, M. A., Ed.	1960	The airflow over mountains. *WMO Tech. Note* **34,** 135 pp. [Available from UNIPUB, 345 Park Avenue South, NY 10010.]
Béland and T. Warn	1975	The radiation condition for transient Rossby waves. *J. Atmos. Sci.*, **32,** 1873–1880.
Bennett, A. F.	1976	Open boundary conditions for dispersive waves. *J. Atmos. Sci.*, **33,** 176–182.
Bougeault, P.	1983	A non-reflective upper boundary condition for limited-height hydrostatic models. *Mon. Wea. Rev.*, **111,** 420–429.
de Boor, C.	1978	*A Practical Guide to Splines*, Springer-Verlag, New York. 392pp.
Durran, D. R., and J. B. Klemp	1983	A compressible model for the simulation of moist mountain waves. *Mon. Wea. Rev.*, **111,** 2341–2361.
Engquist, B., and A. Majda	1977	Absorbing boundary conditions for the numerical simulation of waves. *Math. Comp.*, **31,** 629–651.
Garner, S.	1986	A radiative upper boundary condition adapted for f-plane models. *Mon. Wea. Rev.*, **114,** 1570–1577.
Gill, S.	1951	A process for the step-by-step integration of differential equations in an automatic digital computing machine. *Proc. Camb. Philos. Soc.*, **47,** 96–108.
Givoli, D.	1991	Non-reflecting boundary conditions. *J. Comp. Phys.*, **94,** 78–107.
Hamming, R. W.	1989	*Digital Filters*, Third Edition: Prentice Hall, New Jersey. 284 pp.
Klemp, J. B., and D. Lilly	1978	Numerical simulation of hydrostatic mountain waves. *J. Atmos. Sci.*, **35,** 78–107.
Klemp, J. B., and D. R. Durran	1983	An upper boundary condition permitting internal gravitational wave radiation in numerical mesoscale models. *Mon. Wea. Rev.*, **111,** 430–444.
Morse, P. M., and H. Feshbach	1953	*Methods of Theoretical Physics*, McGraw-Hill. New York. Vol I, 997pp.
Orlanski, I.	1976	A simple boundary condition for unbounded hyperbolic flows. *J. Comput. Phys.*, **21,** 251–269.
Rasch. P. J.	1986	Toward atmospheres without tops; Absorbing upper boundary conditions for numerical models. *Quart. J. Roy. Meteor. Soc.*, **112,** 1195–1218.
Smith, R. B.	1979	The influence of mountains on the atmosphere. Advances in Geophysics, Vol. 21, Academic press, 87–230.

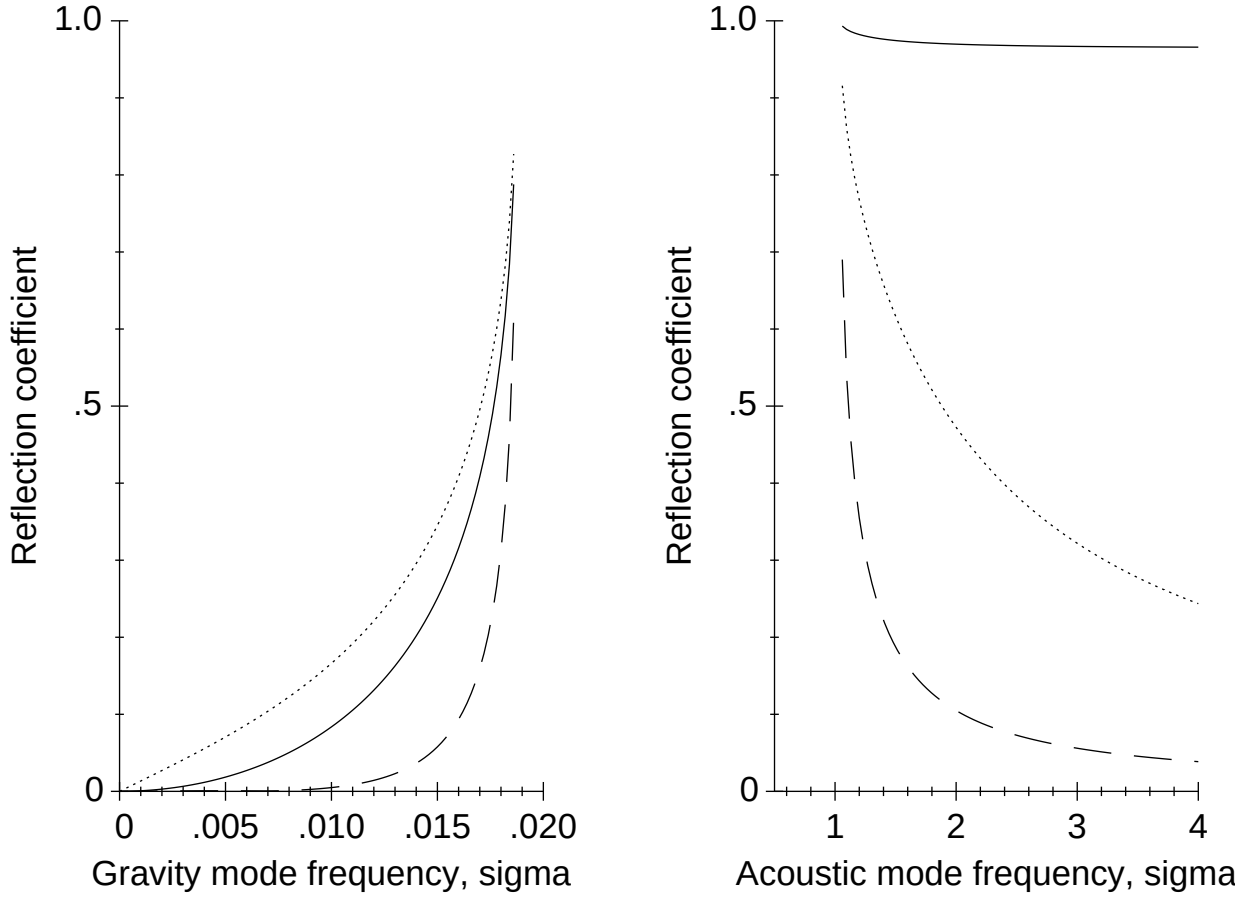

Figure 1. Reflection coefficients for a wave of horizontal wavelength $\lambda = 2000m$ at a variety of frequencies that correspond to gravity or acoustic modes. Solid curves are for the Klemp-Durran and Bougeault condition, $Z = Z_0$; dotted for $Z = Z_1$ with $r = 2s^{-1}$; dashed for $Z = Z_2$ with $b = r/\sqrt{2}$.

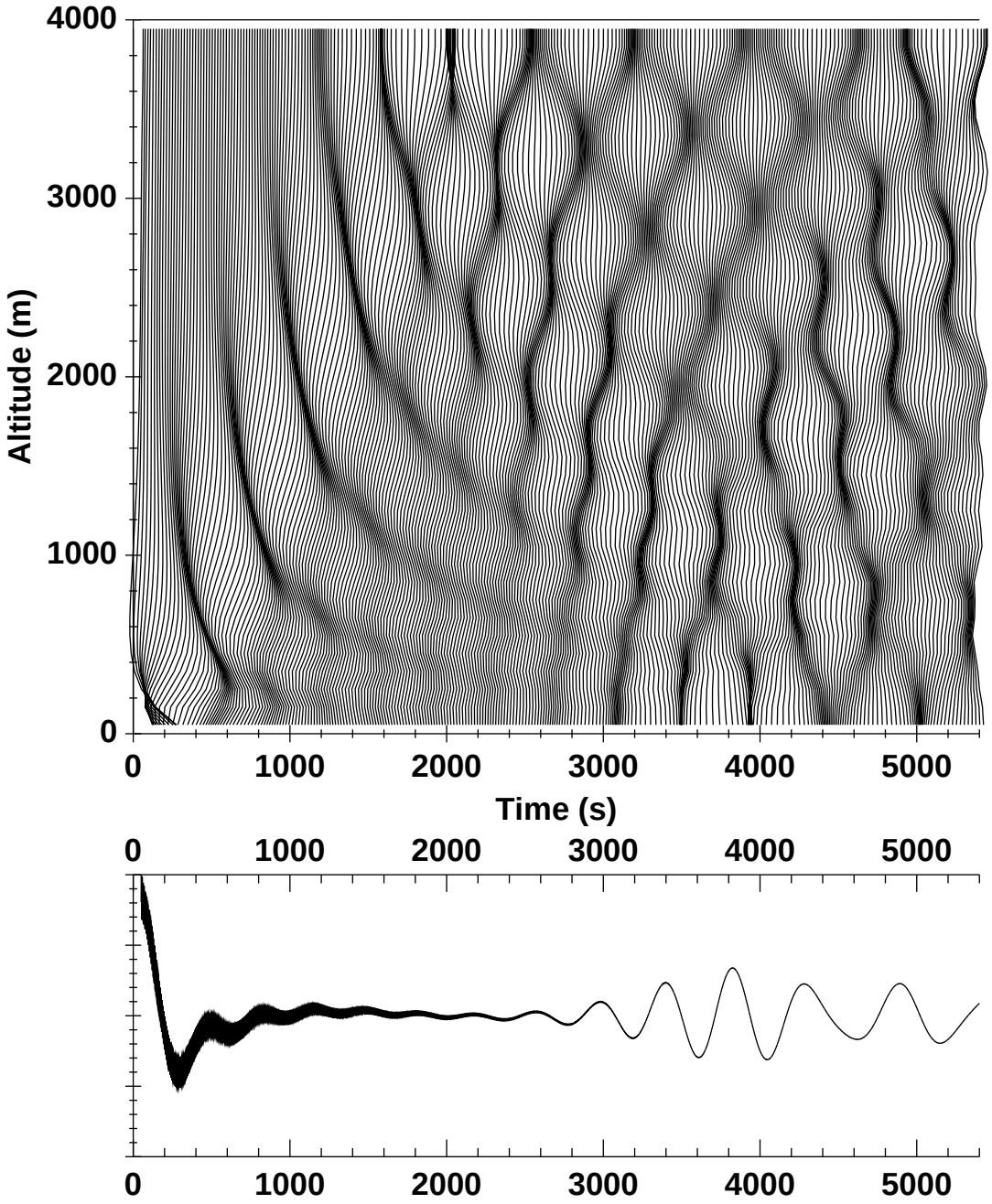

Figure 2. Wave field evolution for the instantaneous impedance condition at the top, $Z(t) = Z_a \delta(0^+)$ in the notation of (3.8), where Z_a is the impedance for acoustic waves. The horizontal wavelength is $\lambda = 2000m$. The upper panel shows multiple profiles of the energy-normalized perturbation of pressure, each profile laterally displaced to accord with the indicated time axis. The lower panel is the graph of the perturbation at the bottom. For clarity, disproportionate amplitudes contemporary with the period of initial forcing are not plotted.

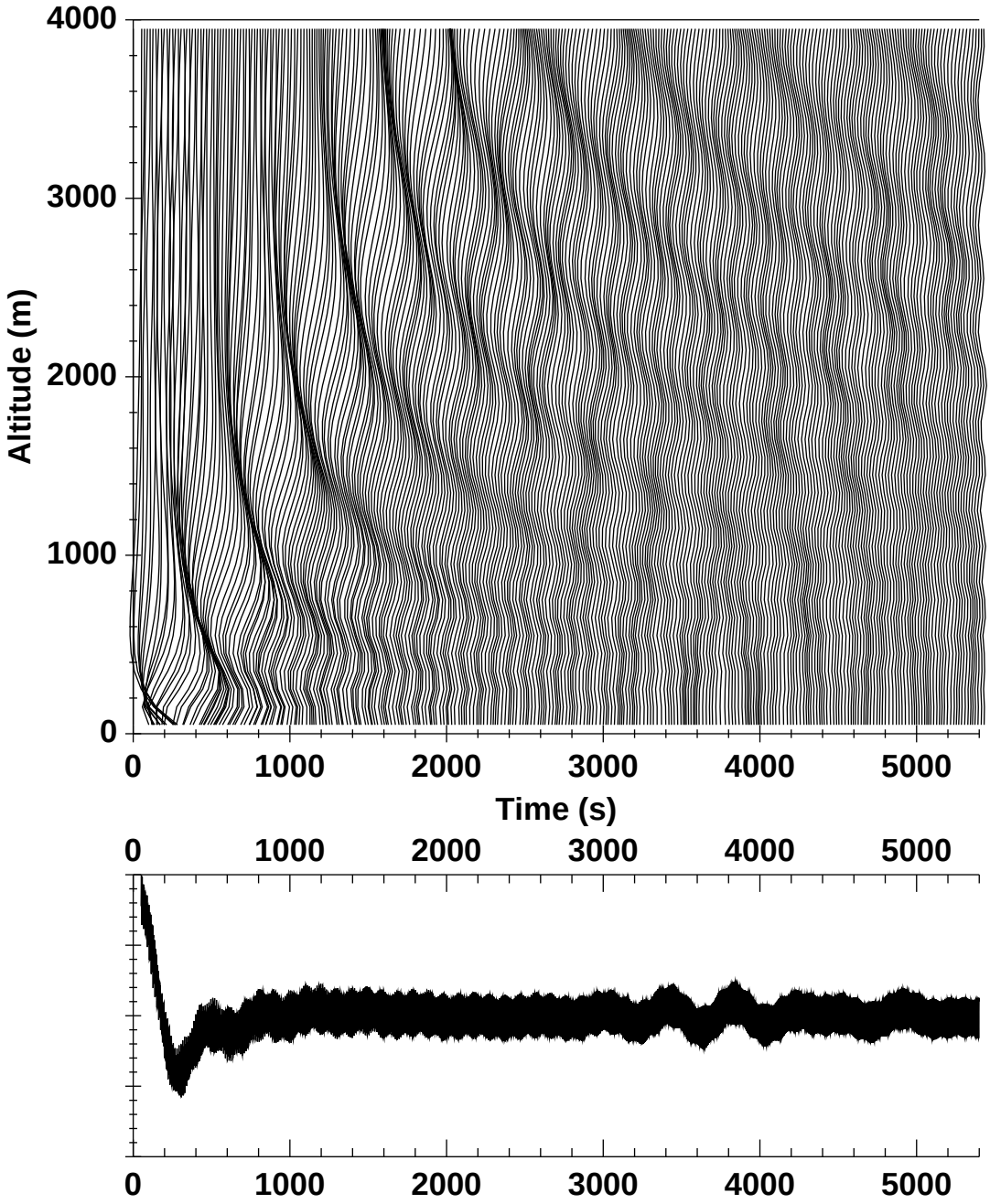

Figure 3. Wave field evolution as in Fig. 2 but with the boundary condition of Klemp and Durran (1983) and Bougeault (1983). This also involves an impulse kernel, but now with $Z(t) = Z_0 \equiv Z_g \delta(0^+)$. As before, $\lambda = 2000m$.

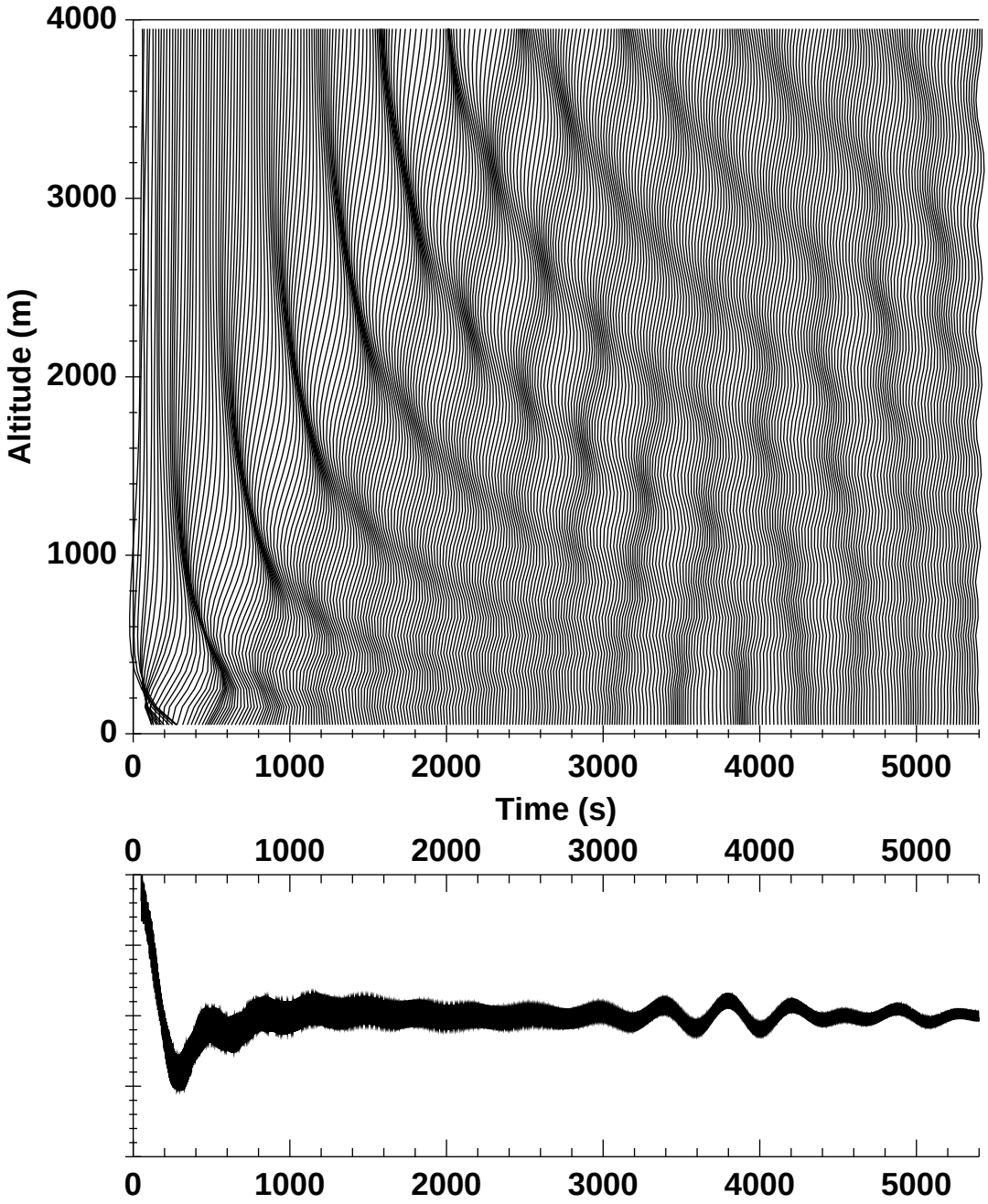

Figure 4. Wave field evolution for the application at the top of the lagged-average impedance condition constructed with the help of a first-order recursive filter, that is, the impedance model referred to in the text by $Z = Z_1$ whose transform is defined by (3.19). The characteristic frequency-scale of the filter used here is $r = 2s^{-1}$. The horizontal wavelength is again $\lambda = 2000m$.

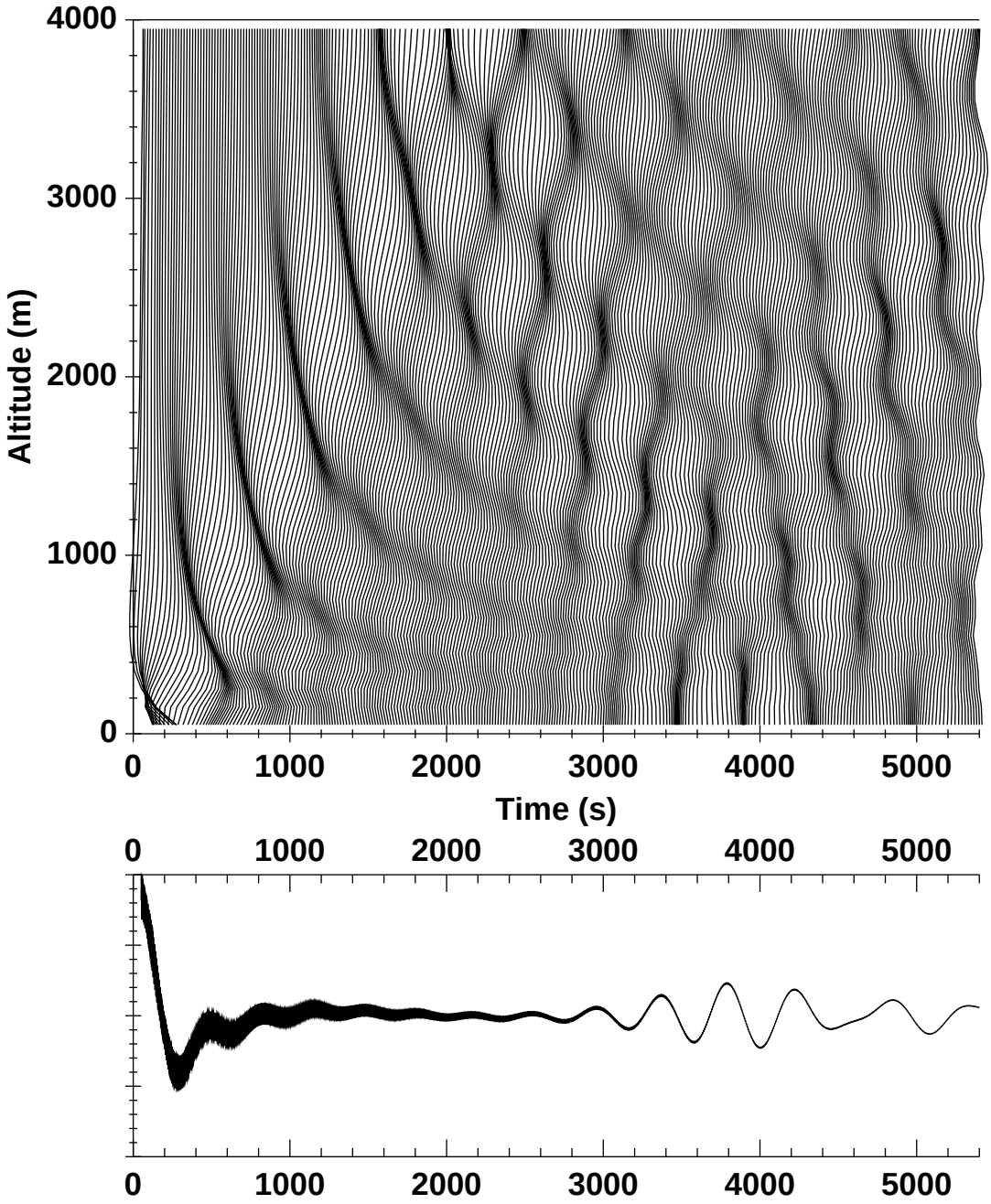

Figure 5. Like Fig. 4, the wave field evolution for $Z = Z_1$, $\lambda = 2000m$ but now with $r = 0.5s^{-1}$. Note that the improvement in the efficiency of removal of acoustic noise is bought at the cost of a less effective radiation condition for the gravity waves.

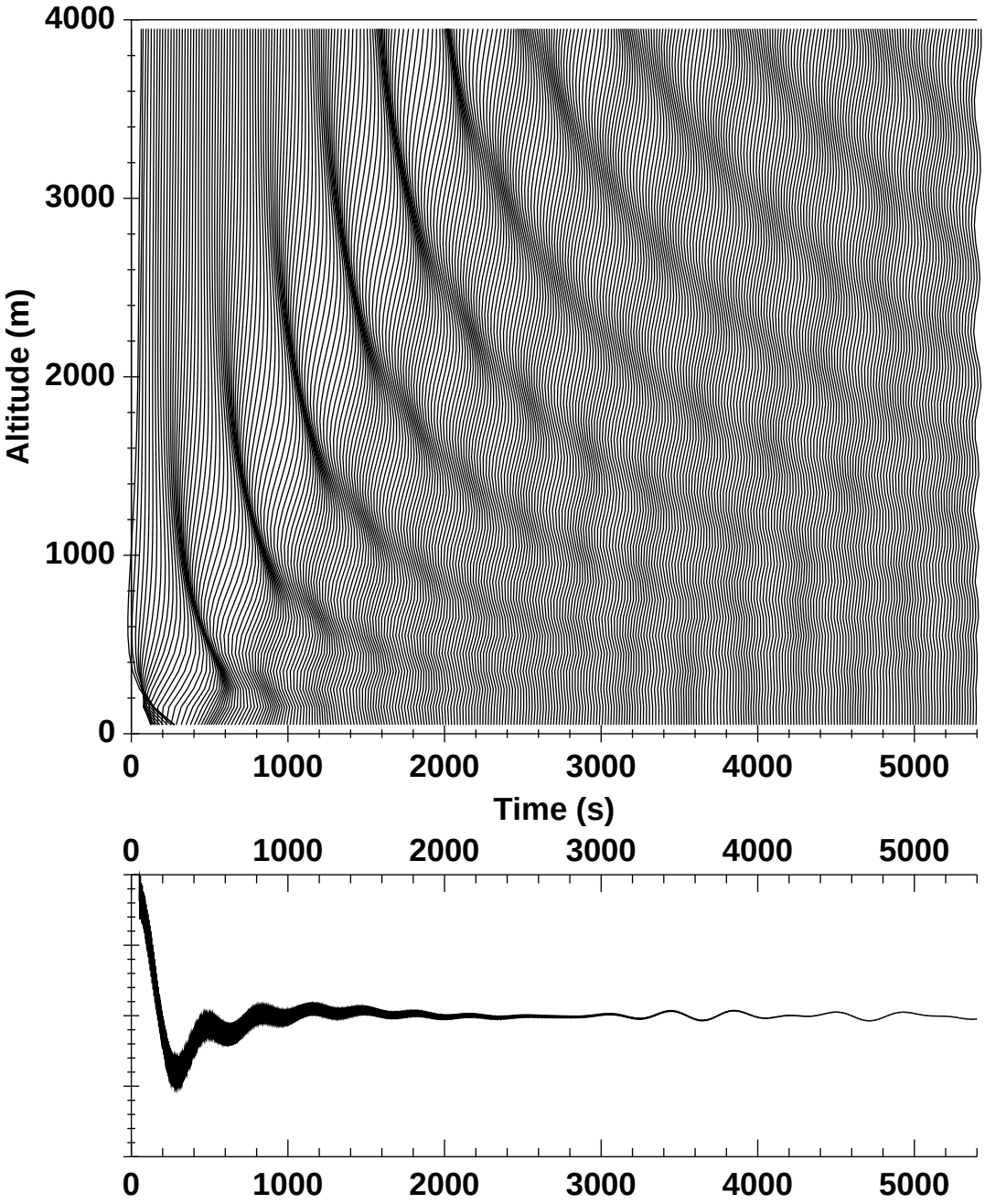

Figure 6. Wave field evolution for the boundary condition employing the second-order filter condition that implies the impedance kernel, $Z = Z_2$, whose transform is defined by (3.20). The horizontal wavelength $\lambda = 2000m$.

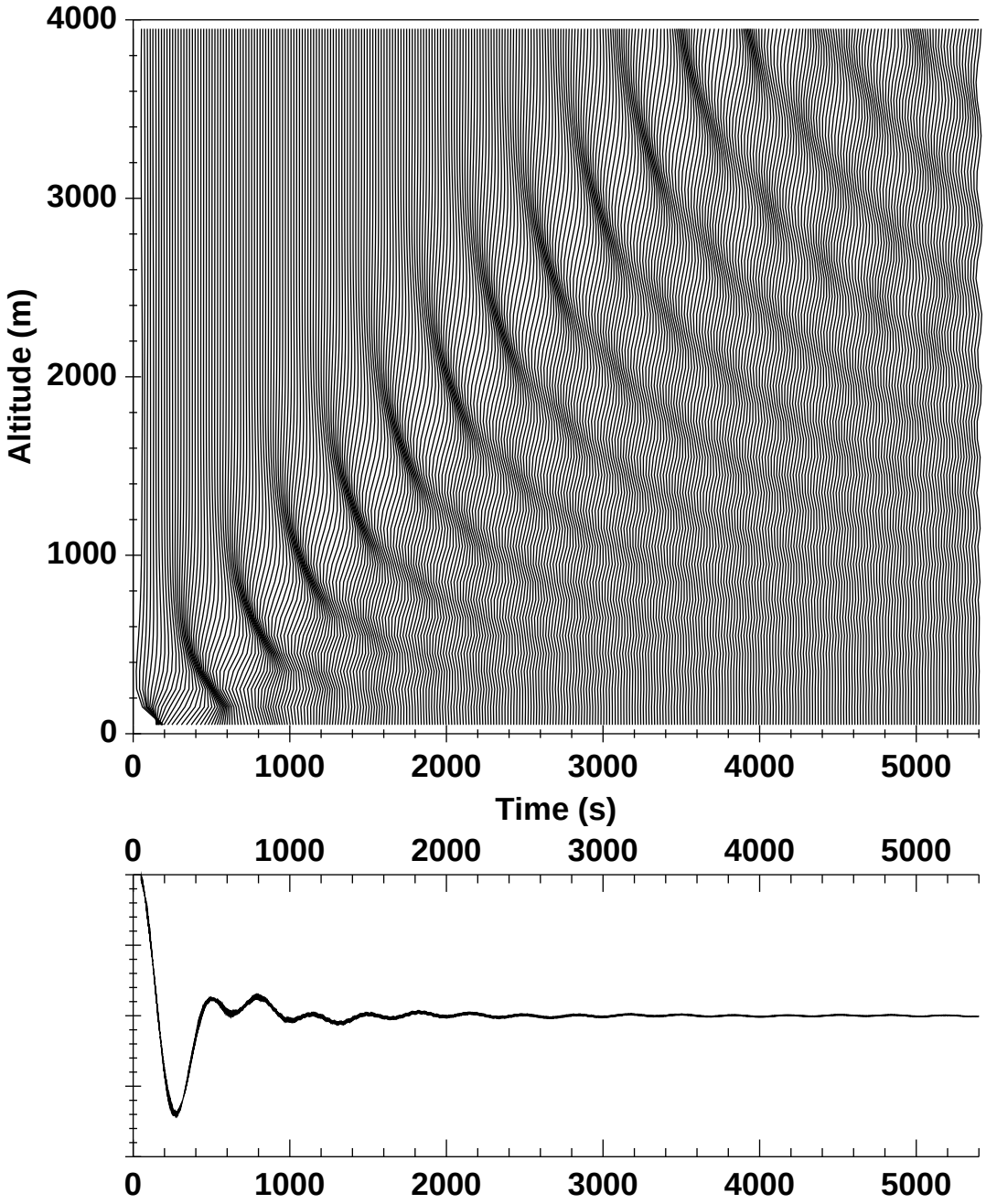

Figure 7. Wave field evolution for $Z = Z_2$ and $\lambda = 1000m$.

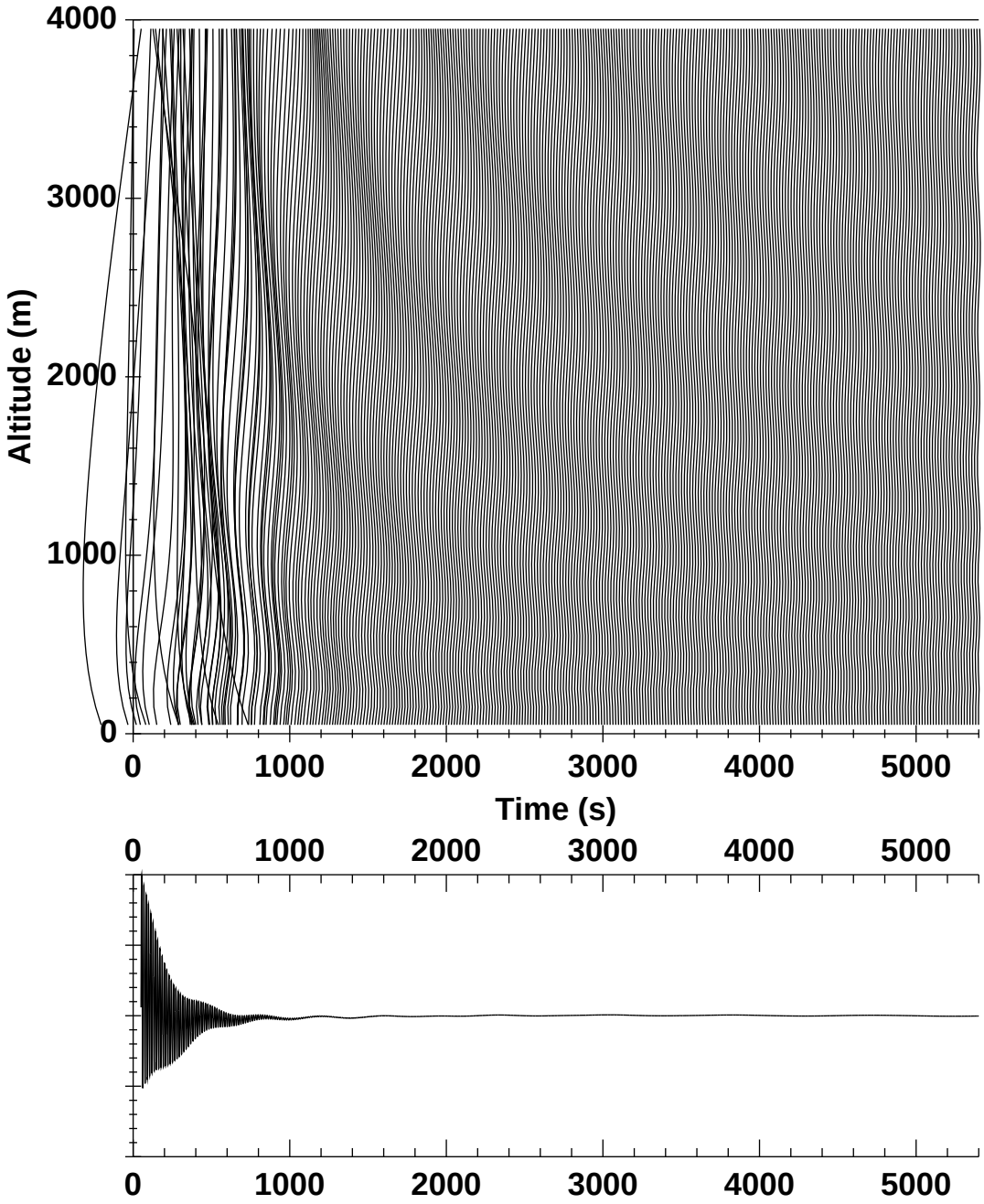

Figure 8. Wave field evolution for $Z = Z_2$ and $\lambda = 5000m$.

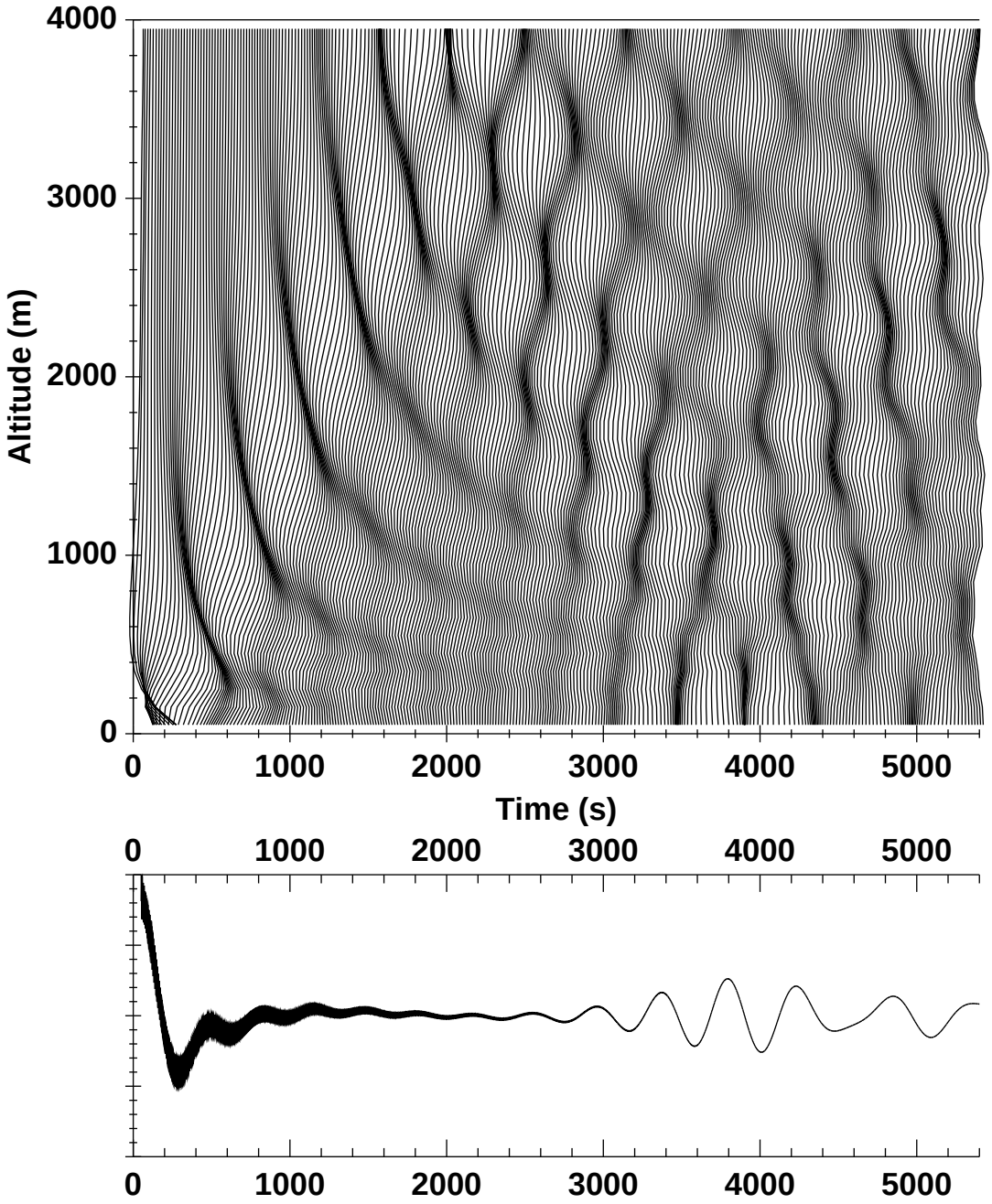

Figure 9. Wave field evolution for $Z = Z_2$ and $\lambda = 2000m$ but modified using $r^2 = c^2k^2/2$ so as to be more efficient for the acoustic end of the spectrum.

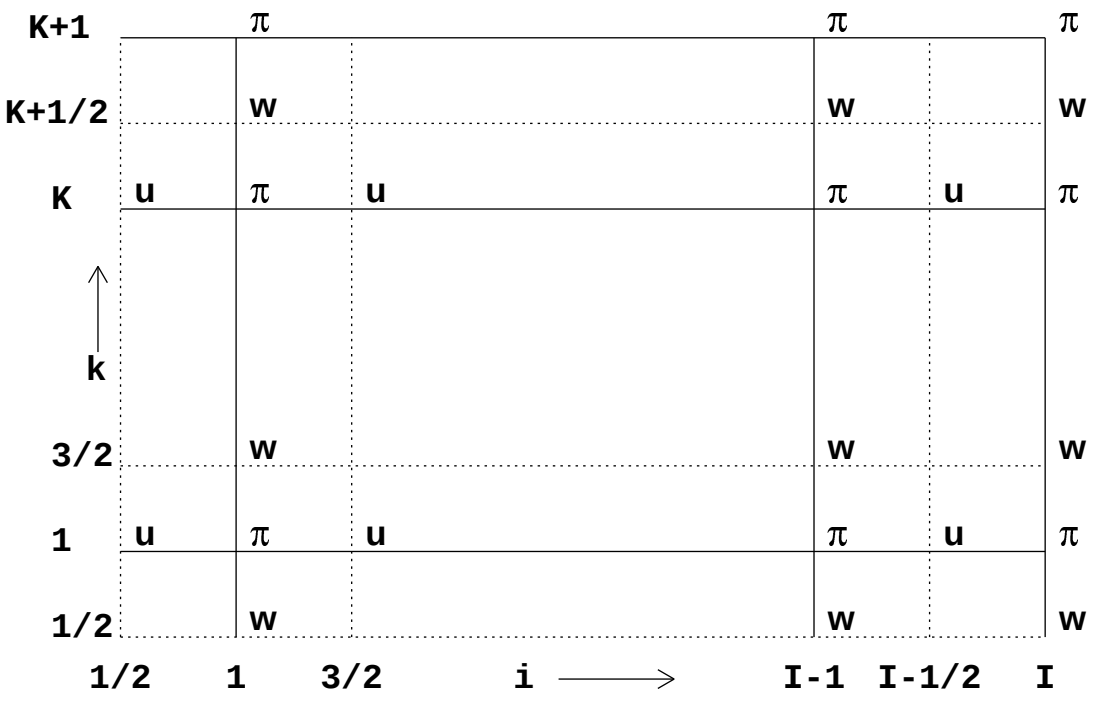

Figure 10. The 2D distribution of model variables on a semi-staggered grid. θ is carried at the same points as w. Here i and k denote the π-grid index in x and the π-level index in z. The prognostic equations are applied everywhere except at the levels $1/2$ and $K+1$. π at the top-most level $K+1$ is diagnosed by the radiation condition.

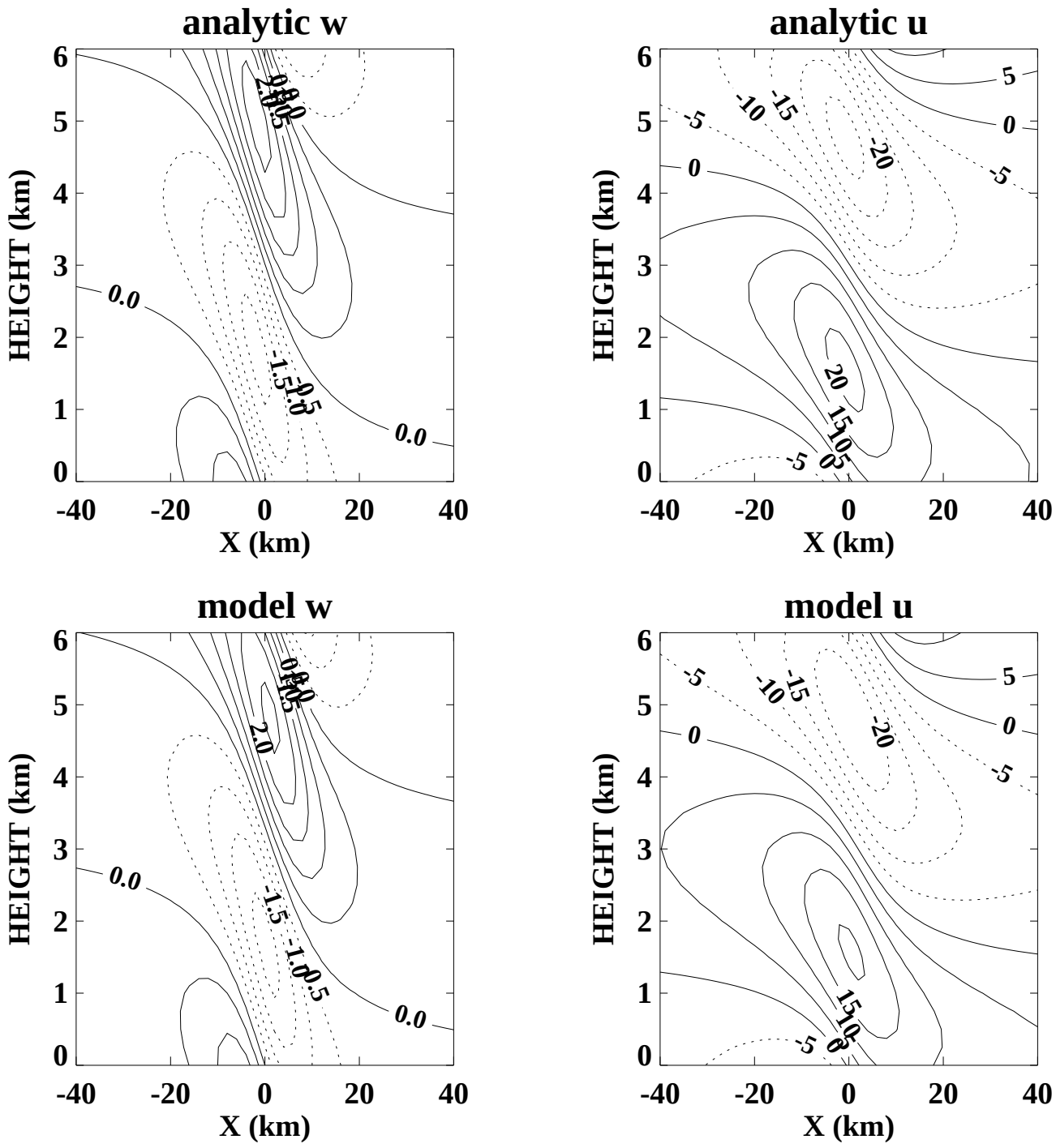

Figure 11. Steady state perturbation vertical and horizontal velocity (m s^{-1}) from the linear hydrostatic solution for a 1 m high mountain. Top two frames are for the analytic solution and the bottom two are for the numerical solution at $u_0 t/a = 60$, the latter solution employs the radiation condition with second-order recursive filter. The perturbations have been multiplied by 1000.

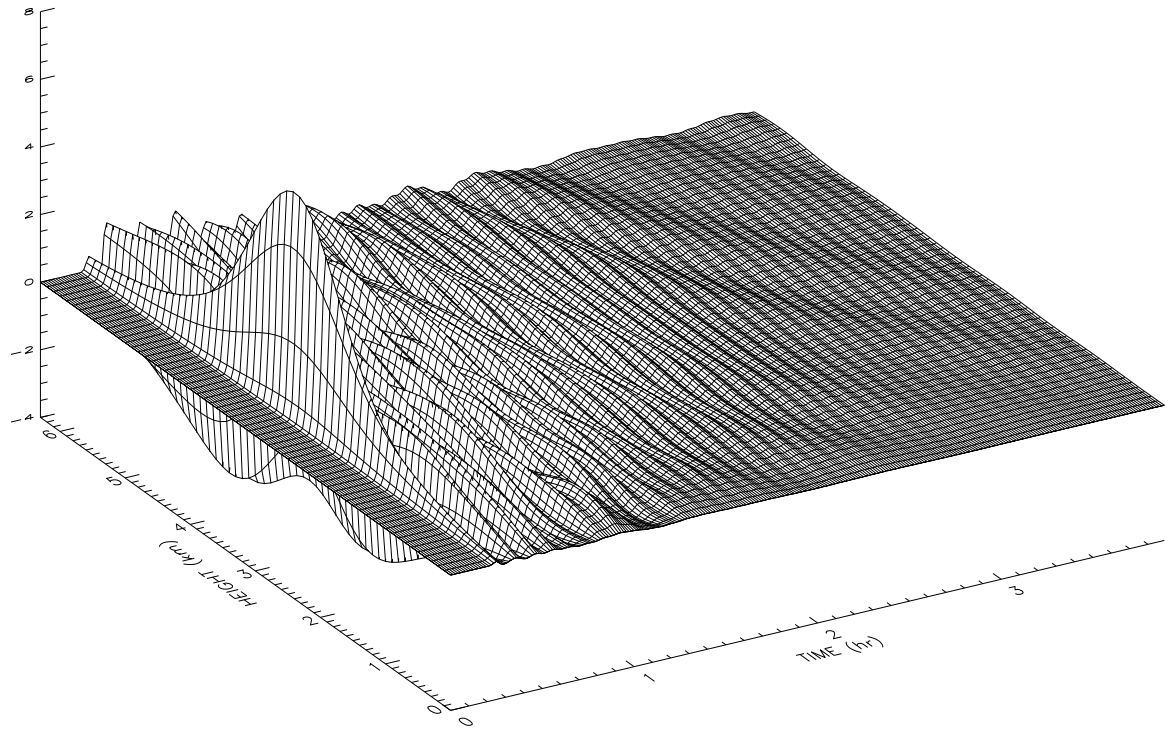

Figure 12. Model simulated perturbation divergence (s^{-1}) as a function of height (km) and time (hr) centered at the π-grid index $i = 64$. The perturbations have been multiplied by 10^9.